

## Optical Manipulation of Bipolarons in a System with Nonlinear Electron-Phonon Coupling

K. Kovač<sup>1</sup>, D. Golež<sup>1,2</sup>, M. Mierzejewski<sup>3</sup>, and J. Bonča<sup>1,2</sup>

<sup>1</sup>*J. Stefan Institute, 1000 Ljubljana, Slovenia*

<sup>2</sup>*Faculty of Mathematics and Physics, University of Ljubljana, 1000 Ljubljana, Slovenia*

<sup>3</sup>*Department of Theoretical Physics, Faculty of Fundamental Problems of Technology, Wrocław University of Science and Technology, 50-370 Wrocław, Poland*

 (Received 4 May 2023; revised 12 September 2023; accepted 13 February 2024; published 4 March 2024)

We investigate full quantum mechanical evolution of two electrons nonlinearly coupled to quantum phonons and simulate the dynamical response of the system subject to a short spatially uniform optical pulse that couples to dipole-active vibrational modes. Nonlinear electron-phonon coupling can either soften or stiffen the phonon frequency in the presence of electron density. In the former case, an external optical pulse tuned just below the phonon frequency generates attraction between electrons and leads to a long-lived bound state even after the optical pulse is switched off. It originates from a dynamical modification of the self-trapping potential that induces a metastable state. By increasing the pulse frequency, the attractive electron-electron interaction changes to repulsive. Two sequential optical pulses with different frequencies can switch between attractive and repulsive interaction. Finally, we show that the pulse-induced binding of electrons is shown to be efficient also for weakly dispersive optical phonons, in the presence anharmonic phonon spectrum and in two dimensions.

DOI: [10.1103/PhysRevLett.132.106001](https://doi.org/10.1103/PhysRevLett.132.106001)

Research in the field of driven quantum materials is at the forefront of modern solid-state physics. The development of new laser sources opened a new chapter in the field [1] where we can selectively excite collective degrees of freedom, like lattice, magnetic, and electronic excitations, to generate new emergent states of matter [2–4]. Among the most prominent examples are optical manipulation of magnetic order [5–8], light-induced nonequilibrium metal-insulator transitions [9–13], and optically enhanced transient states displaying superconducting signatures [2,14–23].

Modifying superconducting transition temperature by external stimulus was first shown using microwave radiation, now known as the Wyatt-Dayem effect [24–26]. More recently, it has been suggested that the selective excitation of a system could dramatically enhance the effect on the electronic system with nonlinear lattice couplings. A classic example includes a nonlinear coupling between optically excited infrared active mode inducing a Raman mode distortion [12,27–29] with modified electronic properties. The idea was applied to cuprate superconductors [30], metal-insulator transition in manganites [9,31] and paraelectric-ferroelectric transition in SrTiO<sub>3</sub> [32,33]. An even more interesting class of scenarios explores the role of quantum mechanical fluctuations on pairing from nonlinear phononics [34]. We expect nonlinear electron-phonon coupling in crystals where light ions are symmetrically intercalated between heavy ions [35] like in organic crystals TMTSF<sub>2</sub>-PF<sub>6</sub> [36] or TTF-TCNQ [37,38]. Recent

experimental realization of strong nonlinear electron-phonon coupling was reported in one dimensional ET-F<sub>2</sub>TCNQ and identified by the presence of strong second harmonics [39,40]. In equilibrium, the nonlinear electron-phonon (EP) coupling leads to light polarons [35] and even more significantly to strongly bound light bipolarons [41]. Out of equilibrium, the squeezed electronic states due to nonlinear electron-lattice coupling can induce attraction between charge carriers inducing either superconducting [42] or insulator-metal transition [43,44]. The second class of ideas is based on the parametric resonance effect, where the interplay of driving and lattice nonlinearities leads to enhanced electron-phonon interaction and pairing [18]. However, other studies point out the competition between pairing, heating, or phonon-induced disorder and, depending on the approximation employed, one or another could prevail [45,46]. Therefore, obtaining exact results for a driven system to understand the competition and gauge which approximations are appropriate for these highly excited correlated states would be highly valuable.

In this Letter, we provide an exact time evolution of a two-electron system coupled nonlinearly to lattice distortions and driven by an external laser pulse, which homogeneously excites dipolar active lattice modes. We show that electronic binding can be dramatically enhanced or reduced depending on the pulse protocol. The electron binding (or repulsion) remains enhanced due to modified bipolaronic self-trapping leading to a long-lived (metastable) state even

after the pulse has been switched off. We show that the binding takes place only for negative values of nonlinear electron-lattice couplings (frequency softening), which is in contrast with previously applied approximation predicting a sign independent binding [18,42,44,46]. Finally, we show that the metastable state slowly decays if Einstein phonons acquire a finite bandwidth, still, the binding remains elevated in comparison to its value before the application of the pulse.

The model under the consideration is given by

$$H_0 = -t_{\text{el}} \sum_{\langle i,j \rangle, s} (c_{i,s}^\dagger c_{j,s} + \text{H.c.}) + g_2 \sum_j \hat{n}_j (a_j^\dagger + a_j)^2 + \omega_0 \sum_j a_j^\dagger a_j + U \sum_j n_{i,\uparrow} n_{i,\downarrow}, \quad (1)$$

where  $\langle i, j \rangle$  represents summation over nearest neighbors,  $c_{j,s}^\dagger$  and  $a_j^\dagger$  are electron and phonon creation operators at site  $j$  and spin  $s$ , respectively,  $\hat{n}_j = \sum_s c_{j,s}^\dagger c_{j,s}$  represents the electron density operator,  $t_{\text{el}}$  the nearest-neighbor electron hopping amplitude, and  $\omega_0$  denotes the Einstein phonon frequency. From here and on we set  $t_{\text{el}} = 1$ . The second term in Eq. (1) represents a quadratic EP coupling, see the Supplemental Material [47] for physical realizations. The last term represents the on-site Coulomb repulsion.

Since the studied Hamiltonian exists in infinitely dimensional Hilbert space one needs to single out a subspace that is relevant for the studied problem. Here, we focus on the dynamics of electrons thus the relevant subspace contains states where multiple phononic excitations may exist in the close proximity of electrons. More distant (in real space) phonon excitations are discarded since they do not influence the distribution of electrons. In order to construct such subspace we have used a numerical method described in detail in Refs. [48–53] as well as in the Supplemental Material [47]. The method contains a single parameter  $N_h$  that determines the maximal distance between electrons as well as the maximal number of phonon excitations.

In the first part we present results for the one-dimensional (1D) case. We excite the system by driving an infrared active mode  $H(t) = H_0 + V(t) \sum_j (a_j^\dagger + a_j)$  with a classical uniform ac field  $V(t) = A_p \sin(\omega_d t) \exp[-(t-t_0)^2/2\sigma^2]$  that couples uniformly to all lattice displacements and time propagate the full problem using the standard Lanczos procedure [54]. Our first observable is the time evolution of the density-density operator

$$\hat{g}(j) = \sum_i \hat{n}_{i,\uparrow} \hat{n}_{i+j,\downarrow}; \quad g(j, t) = \langle \hat{g}(j) \rangle_t, \quad (2)$$

where we use the following notation  $\langle \hat{A} \rangle_t = \langle \psi(t) | \hat{A} | \psi(t) \rangle$ . In the case of two electrons with the opposite spins, the operator  $\hat{g}(j)$  is a projector which singles out states for

which the distance between both electrons equals  $j$  and the average distance between electrons can be obtained as  $\bar{d}(t) = \sum_j |j| g(j, t)$ .

In Fig. 1(a) we present  $g(j, t=0)$  in the initial ground state of the system using a small Coulomb repulsion  $U = 0.5$  that overcomes a weak phonon-mediated attraction. Functional dependence of  $g(j, t=0)$  is consistent with two electrons at an average distance  $\bar{d}(t=0) \sim 6.5$  as also seen from Fig. 1(d). Switching on the pulse  $V(t)$  with a characteristic frequency  $\omega_d/\omega_0 = 0.9$  and different amplitudes  $A_p$  causes the increase of the total and kinetic energies,  $E$  and  $E_{\text{kin}}$ , respectively, and a slight decrease of EP coupling energy  $E_{g_2}$ , see Fig. 1(b). For definitions see the caption of Fig. 1. The increase of  $E$  is predominantly due to the increase of the total number of phonon quanta  $N_{\text{pho}}$ , shown in Fig. 1(c). The most notable effect of the

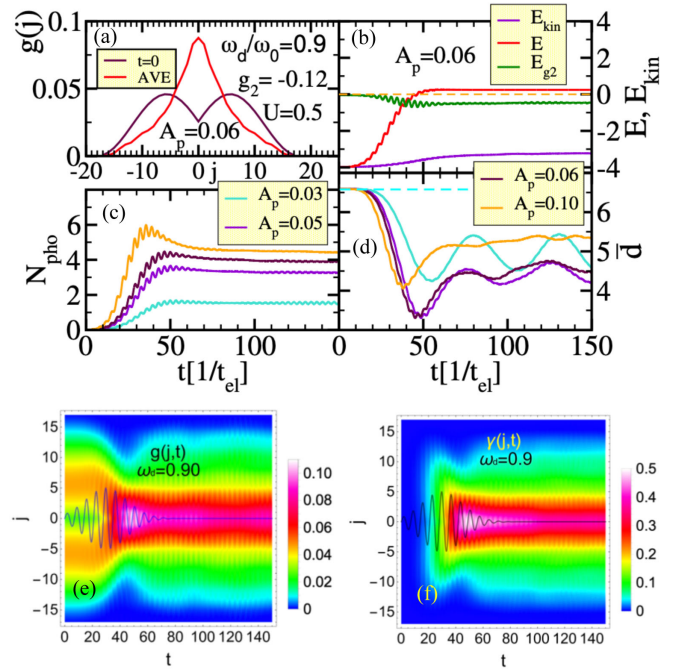


FIG. 1. Different expectation values for 1D system: (a) the density-density correlation function in the ground state  $g(j, t=0)$  and time-averaged  $\bar{g}(j)$  in the time interval [45–150] after the pulse  $V(t)$  with amplitude  $A_p = 0.06$ ,  $\sigma = 15$ ,  $t_0 = 30$ , and frequency  $\omega_d/\omega_0 = 0.9$ ; (b) the total energy  $E(t) = \langle H \rangle_t$ , the kinetic energy  $E_{\text{kin}}(t) = \langle H_{\text{kin}} \rangle_t$  and EP coupling energy  $E_{g_2}(t) = \langle H_{g_2} \rangle_t$  where  $H_{\text{kin}}$  and  $H_{g_2}$  represent the first and the second term in Eq. (1), respectively; (c) the total number of phonon excitations  $N_{\text{pho}} = \langle \sum_j a_j^\dagger a_j \rangle_t$  at different pulse amplitudes  $A_p$ ; (d) the average particle distance  $\bar{d}$ ; (e) the density-density correlation function  $g(j, t)$ ; (f) the number of phonons as a function of the interelectron distance  $\gamma(j, t)$ ; in (e) and (f) we used  $A_p = 0.06$  and the shape of the pulse  $V(t)$  is depicted with a blue line, while its vertical scale is in arbitrary units. In all figures, the driving frequency is  $\omega_d/\omega_0 = 0.9$  and the electron-phonon coupling is  $g_2 = -0.12$ .

pulse is a substantial decrease of the average distance  $\bar{d}$  between electrons, seen in Fig. 1(d). While the increase of  $N_{\text{pho}}$  with increasing  $A_p$  up to  $A_p = 0.08$  is monotonous, the decrease of  $\bar{d}$  is not and the largest drop is achieved around  $A_p \sim 0.06 \pm 0.02$ . The nonmonotonous behavior originates from the competition between the heating effects and the pairing [45]. In Fig. 1(e) the time evolution of the  $g(j, t)$  under the influence of the optical pulse is presented as a density plot conjointly with the time evolution of the pulse,  $V(t)$ . We observe a distinct increase of the double occupancy, given by  $g(0, t)$  that peaks around  $t \sim 40$ . The increased double occupancy persists even long after the pulse has been switched off, creating a very long-lived (metastable) state, which for the case of Einstein phonons persists almost undistorted up to the largest times used in our calculation. This is consistent also with a time-averaged  $\bar{g}(j)$  as seen in Fig. 1(a) displaying a peak at  $j = 0$  in a sharp contrast with its value in the ground state  $g(j, 0)$ . These observations are in a stark contrast to the Floquet-type scenario analyzed in Ref. [18], where the attractive interaction is induced only during the pulse and in the following we will show that it originates from photo-modified self-trapping.

Now, we will explore how the long-lived state emerges due to the substantial absorption of the total energy predominantly stored in the increased number of phonon excitations. It is thus worthwhile determining the distribution of the number of phonons as a function of the relative distance between the electrons  $j$ . It is measured via the time evolution of  $\gamma(j, t) = \langle \hat{\gamma}(j) \rangle_t$ , where

$$\hat{\gamma}(j) = \hat{g}(j) \sum_l a_l^\dagger a_l, \quad (3)$$

describes the total number of phonons in states where the distance between electrons equals  $j$ . As it is shown in Fig. 1(f), most of the excess phonon excitations are absorbed by doubly occupied states, i.e.,  $j = 0$ , and those where electrons are in close proximity. It seems as if the excess phonon excitations represent the *glue* that at least for the given driving frequency  $\omega_d/\omega_0 = 0.9$  provides a self-trapped attractive potential.

Searching further for the origin of the optically induced electron-electron potential we realize that it can only originate from the nonlinear electron-phonon interaction term in Eq. (1), i.e., from the term  $H_{g_2} = g_2 \sum_j \hat{n}_j (a_j^\dagger + a_j)^2$ . We define an effective potential by projecting  $H_{g_2}$  on a subspace with a specified distance between electrons:

$$\hat{v}(j) = \hat{g}(j) H_{g_2}, \quad (4)$$

which yields the time evolution of the effective potential  $v(j, t) = \langle \hat{v}(j) \rangle_t$ . This definition is further justified by the sum rule that gives the total interacting energy  $\sum_j v(j, t) = E_{g_2}(t)$  shown in Fig. 1(b).

Motivated by previous Floquet analysis [18] and a driven atomic limit analysis, see Supplemental Material [47], predicting attractive (repulsive) electronic interaction for driving below (above) lattice frequency, we present  $v(j, t)$  for two distinct driving frequencies leading to attractive  $\omega_d/\omega_0 = 0.9$  and repulsive  $\omega_d/\omega_0 = 1.1$  interaction for  $g_2 = -0.12$ , see Figs. 2(a) and 2(b). When  $\omega_d/\omega_0 = 0.9$  the pulse generates a pronounced peak located at  $j = 0$ , signaling the attractive effective potential that is most negative for the doubly occupied site. This is also presented in Fig. 2(c) where we show time averaged  $\bar{v}(j)$ . In contrast, at  $\omega_d/\omega_0 = 1.1$ , two minima appear around  $j \pm 10$  that are further apart than the shallow minima in the ground state at  $t = 0$ , most clearly observed in Fig. 2(c). This is consistent with repulsive interaction considering that our computations are performed on a finite-size system. In Fig. 2(d) we further investigate the dependence of the effective potential on  $\omega_d$ . We present time-averaged  $\bar{v}(j)$  computed using different driving frequencies  $\omega_d$ . While the strongest attractive interaction is observed around  $\omega_d/\omega_0 = 0.9$ , with increasing  $\omega_d$  the minimum at  $j = 0$  splits into two separate minima, consistent with the onset of a repulsive interaction. Around  $\omega_d/\omega_0 = 1.1$  the separation of the local minima reaches its largest value  $|j| \sim 10$ . With further increase of  $\omega_d$  the depth of the local minima diminishes and merges with the background. The presence of the minima after the pulse is in a clear distinction with the Floquet analysis, where the response is present only during the

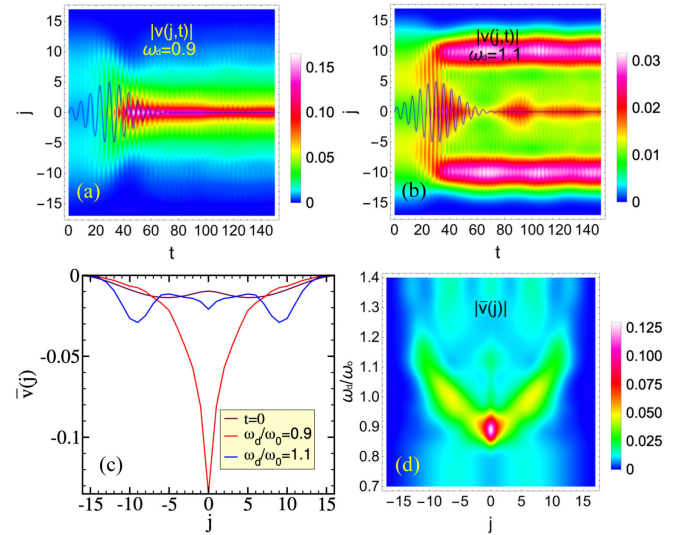


FIG. 2. (a) and (b) Magnitude of the effective potential  $|v(j, t)|$  computed with two distinct driving frequencies  $\omega_d/\omega_0 = 0.9$  and  $1.1$ , respectively. Note that the sign of  $v(j, t)$  is strictly negative since  $g_2 = -0.12$ ; (c) the effective potential in the ground state,  $v(j, 0)$ , and time-averaged  $\bar{v}(j)$  for two distinct  $\omega_d$ . Time averages were performed in the same interval as in Fig. 1(a); (d) time-averaged  $\bar{v}(j)$  for different  $\omega_d$ . We have used the pulse amplitude  $A_p = 0.06$  while the other parameters are identical to those used in Fig. 1.

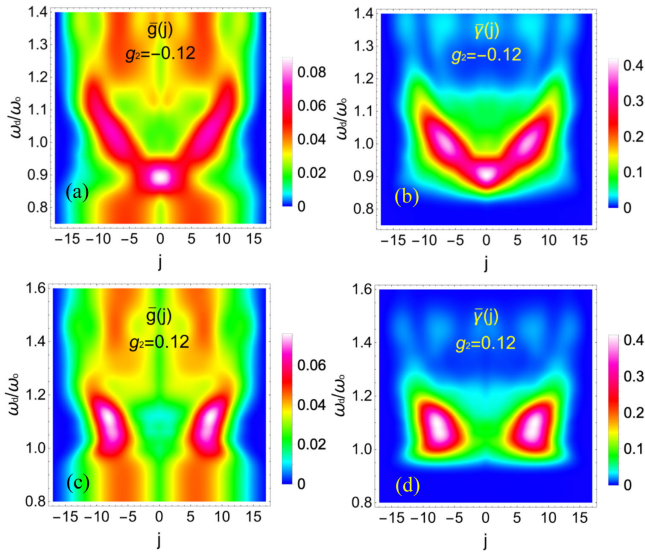


FIG. 3. (a) and (c) The time-averaged density-density correlation function  $\bar{g}(j)$  computed using different driving frequencies  $\omega_d$  for  $g_2 = -0.12$  and  $0.12$ , respectively; (b) and (d) Time-averaged phonon distribution function  $\bar{\gamma}(j)$ . In all cases the time averages were performed in the same interval as in Figs. 1(a) and 2(d). We have used the pulse amplitude  $A_p = 0.06$  while the rest of parameters are identical to those used in Fig. 1.

pulse. The dynamics of  $v(j)$  shows that this interaction originates from the dynamical modification of the trapping potential leading to a long-lived state.

To obtain a deeper insight into this phenomenon we compute the time-averaged  $\bar{g}(j)$  and the time-averaged  $\bar{\gamma}(j)$  and perform a scan over  $\omega_d$  at  $g_2 = -0.12$ , see Figs 3(a) and 3(b), respectively. For  $\omega_d/\omega_0 \lesssim 0.8$  and  $\omega_d/\omega_0 \gtrsim 1.3$ ,  $\bar{g}(j)$  resembles its value in the ground state before the pulse has been switched on. This is consistent with the lack of the absorbed energy from the pulse as seen in Fig. 3(b) where we observe only a tiny amount of excess phonon excitations in the same  $\omega_d$  regime. Near  $\omega_d/\omega_0 \sim 0.9$ ,  $\bar{g}(j)$  shows a pronounced maximum due to an increased weight of doubly occupied states ( $j = 0$ ) consistent with an attractive electron-electron interaction. With increasing  $\omega_d$  the attractive nature of interactions switches towards a repulsive one as the maximum of  $\bar{g}(j)$  moves towards larger values of  $j$ . At  $\omega_d/\omega_0 \sim 1.1$  the maximal value of  $\bar{g}(j)$  appears around  $j \sim \pm 10$  that exceeds its average value in the ground state signaling a strengthening of the repulsive interaction.

The evolution of  $\bar{g}(j)$  caused by changing driving frequencies  $\omega_d$  is closely followed by the evolution of the absorbed phonon excitation distributions,  $\bar{\gamma}(j)$ , shown in Fig. 3(b). It is crucial to stress that time averages are performed in the regime where the optical pulse  $V(t)$  that couples to all oscillators has been switched off. When the pulse is off-resonance, i.e., when  $\omega_d/\omega_0 \gg 1$  or  $\omega_d/\omega_0 \ll 1$ , the system does not absorb much energy; consequently,  $\bar{\gamma}(j) \sim 0$  and  $\bar{g}(j)$  remains close to its ground

state value. It is worth pointing out that the maximum in the absorbed energy, presented in Fig. 3(b), appears at  $\omega_d/\omega_0 \sim 0.96$  which is just above the value  $\omega_d/\omega_0 \sim 0.9$  where maximal attractive interaction is observed. All this analysis shows that exactly at the resonance the heating effect dominates, but slightly below (above) the binding (repulsion) can win and remarkably leads to a very long-lived state due to the self-trapping mechanism. Remarkably, we observe that the self-trapping potential can be reversed by two successive optical pulses which can switch between attractive and repulsive electron-electron interactions, see Supplemental Material [47].

In Figs. 3(c) and 3(d) we show results for positive  $g_2 = 0.12$ . Absorption of energy from the pulse appears at higher  $\omega_d$  then in the case when  $g_2 < 0$ , which is consistent with the increase of the phonon frequency in the presence of finite electron density for  $g_2 > 0$ . In contrast to the  $g_2 < 0$  case, the absorption of energy always leads to repulsive interaction. The observation contrasts with previous analysis [18,42,44,46] based on the atomic limit or perturbative arguments, which predicted sign-independent pairing. Suppose this observation survives beyond the dilute limit. In that case, it poses a strong constraint on materials where we can expect light-induced long-lived attractive interaction due to the nonlinear electron-lattice couplings.

Now, we address how robust is the metastable state to various perturbations. In Supplemental Material [47], we show the resilience to the presence of the linear EP coupling term, phonon dispersion, anharmonic effects, and next-nearest-neighbor hopping term. An important remaining question is whether the optically induced attraction survives in higher dimensions and we will demonstrate it for the two-dimensional (2D) case of Eq. (1). The model can describe nonlinear coupling to phonon modes that are perpendicular to the plane. The system is defined on an infinite 2D plane, taking into account translational symmetry while the maximal distance between electrons is given by  $N_h$  and the maximal number of phonons in the system is  $N_h - 1$  [48,49].

Figure 4(a) shows the ground state density-density correlation function  $g(x, y, t = 0)$ , where  $g(x, y, t) = \sum_{x', y'} \langle \hat{n}_{(x', y'), \uparrow} \hat{n}_{(x'+x, y'+y), \downarrow} \rangle_t$  at  $g_2 = -0.12$ . Because of the presence of nonzero  $U = 0.5$  there is a shallow local minimum at the center, presenting the doubly occupied site;  $x = y = 0$ . Note also that  $g(x, y, t)$  is normalized, i.e.,  $\sum_{x, y} g(x, y, t) = 1$ , it therefore represents the probability for a state where the relative position of the electrons is given by  $(x, y)$ . In Fig. 4(b) we present time-averaged  $\bar{g}(x, y)$  after driving. The size of the bipolaron as a result of driving shrinks while the probability for double occupation increases. This is more quantitatively shown in Fig. 4(c) where the average distance  $\bar{d}(t)$  shows a substantial decrease during as well as after the driving.

In conclusion, we have performed numerically exact time evolution of a bipolaron problem coupled by a

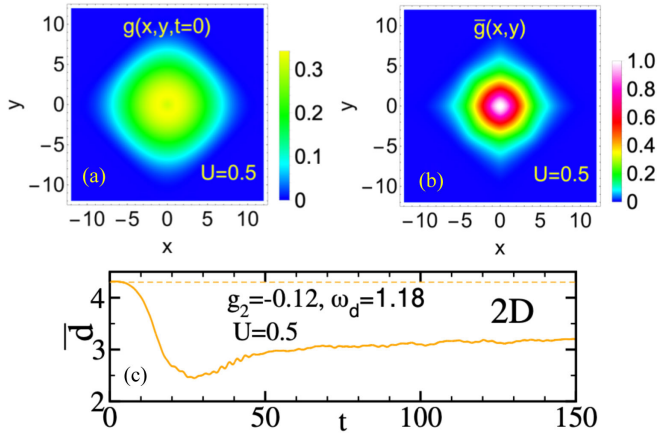


FIG. 4. (a)  $g(x, y, t=0)$  computed in the ground state at  $\omega_0 = 1$ ,  $g_2 = -0.12$  for the 2D version of the model in Eq. (1); (b) Time-averaged  $\bar{g}(x, y)$  where time averages have been performed in the time interval  $t \in [45, 150]$ ; to facilitate comparison between results computed before and after driving, we have rescaled the density plots so that the largest value of  $\bar{g}(x, y)$  is set to unity; (c) the average distance between particles  $\bar{d}(t) = \sum_{x,y} \sqrt{x^2 + y^2} g(x, y, t)$ . We have used  $N_h = 12$  while the size of the Hilbert space was  $N_{\text{st}}^{2D} \sim 2.6 \times 10^6$  and the rest of parameters of the model are the same as in the 1D case. For the driving field we have used the following parameters  $\omega_d/\omega_0 = 1.18$ ,  $A = 0.1$ ,  $\sigma = 15$ ,  $t_0 = 30$ .

nonlinear electron-phonon interaction. When the electron-lattice interaction leads to phonon softening  $g_2 < 0$ , a properly tuned uniform optical pulse that couples to dipole-active lattice vibrations may optically induce either attractive or repulsive interaction between electrons. Here the primary mechanism originates from strong dependence of the effective phonon frequency on the local density of electrons [42] so that an appropriately tuned pulse excites phonons corresponding to specific configurations of electrons. In one dimension the strongest attractive interaction appears when pulses are tuned slightly below the Einstein phonon frequency  $\omega_0$ . This suggests that a softening of the lattice vibration due to an increased electron density and double occupancy plays an essential role in the appearance of the attractive potential between electrons. In contrast, a driving frequency slightly exceeding  $\omega_0$  generates repulsive interaction. In both cases, the effects of optically induced interactions persist long after the pulse has been switched off. Since the energy of the phonon subsystem depends on the density of electrons, both subsystems build an effective trap potential that mutually stabilizes the spatial configurations of electrons and phonons. We have demonstrated that optically induced interaction survives under various perturbations of the original Hamiltonian, such as the introduction of weakly dispersive phonons, anharmonic effects on phonon frequency spectrum, and the introduction of the linear EP coupling. The mechanism is stable also in

two and possibly also in higher dimensions. An important future problem is extending the bipolaron problem to finite doping to understand if we can induce coherence between these highly excited composite particles and to explore the experimental consequences of such states.

J. B., D. G., and K. K. acknowledge the support by the program No. P1-0044 of the Slovenian Research Agency (ARRS). Additionally, D. G. acknowledges the support from the programs MN-0016-106 and No. J1-2455 of the Slovenian Research Agency (ARRS). J. B. acknowledges discussions with S. A. Trugman, A. Saxena, and support from the Center for Integrated Nanotechnologies, a U.S. Department of Energy, Office of Basic Energy Sciences user facility and Physics of Condensed Matter and Complex Systems Group (T-4) at Los Alamos National Laboratory. M. M. acknowledges support by the National Science Centre, Poland via Project No. 2020/37/B/ST3/00020.

- 
- [1] D. N. Basov, R. D. Averitt, and D. Hsieh, *Nat. Mater.* **16**, 1077 (2017).
  - [2] C. Giannetti, M. Capone, D. Fausti, M. Fabrizio, F. Parmigiani, and D. Mihailovic, *Adv. Phys.* **65**, 58 (2016).
  - [3] P. Salén, M. Basini, S. Bonetti, J. Hebling, M. Krasilnikov, A. Y. Nikitin, G. Shamuilov, Z. Tibai, V. Zhaunerchyk, and V. Goryashko, *Phys. Rep.* **836–837**, 1 (2019).
  - [4] A. dela Torre, D. M. Kennes, M. Claassen, S. Gerber, J. W. McIver, and M. A. Sentef, *Rev. Mod. Phys.* **93**, 041002 (2021).
  - [5] A. Kirilyuk, A. V. Kimel, and T. Rasing, *Rev. Mod. Phys.* **82**, 2731 (2010).
  - [6] M. Först, R. I. Tobey, S. Wall, H. Bromberger, V. Khanna, A. L. Cavalieri, Y.-D. Chuang, W. S. Lee, R. Moore, W. F. Schlotter *et al.*, *Phys. Rev. B* **84**, 241104(R) (2011).
  - [7] J. H. Mentink, K. Balzer, and M. Eckstein, *Nat. Commun.* **6**, 6708 (2015).
  - [8] T. F. Nova, A. Cartella, A. Cantaluppi, M. Först, D. Bossini, R. V. Mikhaylovskiy, A. V. Kimel, R. Merlin, and A. Cavalleri, *Nat. Phys.* **13**, 132 (2017).
  - [9] M. Rini, R. Tobey, N. Dean, J. Itatani, Y. Tomioka, Y. Tokura, R. W. Schoenlein, and A. Cavalleri, *Nature (London)* **449**, 72 (2007).
  - [10] H. Okamoto, H. Matsuzaki, T. Wakabayashi, Y. Takahashi, and T. Hasegawa, *Phys. Rev. Lett.* **98**, 037401 (2007).
  - [11] S. Kaiser, S. R. Clark, D. Nicoletti, G. Cotugno, R. I. Tobey, N. Dean, S. Lupi, H. Okamoto, T. Hasegawa, D. Jaksch *et al.*, *Sci. Rep.* **4**, 3823 (2014).
  - [12] A. Subedi, A. Cavalleri, and A. Georges, *Phys. Rev. B* **89**, 220301(R) (2014).
  - [13] L. Stojchevska, I. Vaskivskiy, T. Mertelj, P. Kusar, D. Svetin, S. Brazovskii, and D. Mihailovic, *Science* **344**, 177 (2014).
  - [14] D. Fausti, R. I. Tobey, N. Dean, S. Kaiser, A. Dienst, M. C. Hoffmann, S. Pyon, T. Takayama, H. Takagi, and A. Cavalleri, *Science* **331**, 189 (2011).

- [15] W. Hu, S. Kaiser, D. Nicoletti, C. R. Hunt, I. Gierz, M. C. Hoffmann, M. Le Tacon, T. Loew, B. Keimer, and A. Cavalleri, *Nat. Mater.* **13**, 705 (2014).
- [16] M. Mitrano, A. Cantaluppi, D. Nicoletti, S. Kaiser, A. Perucchi, S. Lupi, P. Di Pietro, D. Pontiroli, M. Riccò, S. R. Clark *et al.*, *Nature (London)* **530**, 461 (2016).
- [17] M. Knap, M. Babadi, G. Refael, I. Martin, and E. Demler, *Phys. Rev. B* **94**, 214504 (2016).
- [18] M. Babadi, M. Knap, I. Martin, G. Refael, and E. Demler, *Phys. Rev. B* **96**, 014512 (2017).
- [19] A. F. Kemper, M. A. Sentef, B. Moritz, T. P. Devereaux, and J. K. Freericks, *Ann. Phys. (Berlin)* **529**, 1600235 (2017).
- [20] G. Mazza and A. Georges, *Phys. Rev. B* **96**, 064515 (2017).
- [21] N. Bittner, T. Tohyama, S. Kaiser, and D. Manske, *J. Phys. Soc. Jpn.* **88**, 044704 (2019).
- [22] A. Grankin, M. Hafezi, and V. M. Galitski, *Phys. Rev. B* **104**, L220503 (2021).
- [23] M. Buzzi, D. Nicoletti, M. Fechner, N. Tancogne-Dejean, M. A. Sentef, A. Georges, T. Biesner, E. Uykur, M. Dressel, A. Henderson *et al.*, *Phys. Rev. X* **10**, 031028 (2020).
- [24] A. F. G. Wyatt, V. M. Dmitriev, W. S. Moore, and F. W. Sheard, *Phys. Rev. Lett.* **16**, 1166 (1966).
- [25] A. H. Dayem and J. J. Wiegand, *Phys. Rev.* **155**, 419 (1967).
- [26] G. M. Eliashberg, *JETP Lett.* **11**, 186 (1970).
- [27] M. Först, C. Manzoni, S. Kaiser, Y. Tomioka, Y. Tokura, R. Merlin, and A. Cavalleri, *Nat. Phys.* **7**, 854 (2011).
- [28] A. S. Disa, T. F. Nova, and A. Cavalleri, *Nat. Phys.* **17**, 1087 (2021).
- [29] A. Subedi, *C.R. Phys.* **22**, 161 (2021).
- [30] R. Mankowsky, A. Subedi, M. Först, S. O. Mariager, M. Chollet, H. Lemke, J. S. Robinson, J. M. Glownia, M. P. Minitti, A. Frano *et al.*, *Nature (London)* **516**, 71 (2014).
- [31] V. Esposito, M. Fechner, R. Mankowsky, H. Lemke, M. Chollet, J. M. Glownia, M. Nakamura, M. Kawasaki, Y. Tokura, U. Staub *et al.*, *Phys. Rev. Lett.* **118**, 247601 (2017).
- [32] A. Subedi, *Phys. Rev. B* **95**, 134113 (2017).
- [33] T. Nova, A. Disa, M. Fechner, and A. Cavalleri, *Science* **364**, 1075 (2019).
- [34] D. E. Kiselov and M. V. Feigel'man, *Phys. Rev. B* **104**, L220506 (2021).
- [35] C. P. J. Adolphs and M. Berciu, *Phys. Rev. B* **89**, 035122 (2014).
- [36] M. Kaveh, M. Weger, and L. Friedman, *Phys. Rev. B* **26**, 3456 (1982).
- [37] H. Gutfreund and M. Weger, *Phys. Rev. B* **16**, 1753 (1977).
- [38] O. Entin-Wohlman, H. Gutfreund, and M. Weger, *J. Phys. C* **18**, L61 (1985).
- [39] S. Kaiser, S. Clark, D. Nicoletti, G. Cotugno, R. Tobey, N. Dean, S. Lupi, H. Okamoto, T. Hasegawa, D. Jaksch *et al.*, *Sci. Rep.* **4**, 3823 (2014).
- [40] R. Singla, G. Cotugno, S. Kaiser, M. Först, M. Mitrano, H. Y. Liu, A. Cartella, C. Manzoni, H. Okamoto, T. Hasegawa *et al.*, *Phys. Rev. Lett.* **115**, 187401 (2015).
- [41] C. P. J. Adolphs and M. Berciu, *Phys. Rev. B* **90**, 085149 (2014).
- [42] D. M. Kennes, E. Y. Wilner, D. R. Reichman, and A. J. Millis, *Nat. Phys.* **13**, 479 (2017).
- [43] F. Grandi, J. Li, and M. Eckstein, *Phys. Rev. B* **103**, L041110 (2021).
- [44] M. A. Sentef, *Phys. Rev. B* **95**, 205111 (2017).
- [45] Y. Murakami, N. Tsuji, M. Eckstein, and P. Werner, *Phys. Rev. B* **96**, 045125 (2017).
- [46] J. Sous, B. Kloss, D. M. Kennes, D. R. Reichman, and A. J. Millis, *Nat. Commun.* **12**, 5803 (2021).
- [47] See Supplemental Material at <http://link.aps.org/supplemental/10.1103/PhysRevLett.132.106001> for the description of the numerical method, resilience of the metastable state to various perturbations, results obtained with the driving frequency  $\omega_d/\omega_0 = 1.1$ , the response of the system for  $g_2 = 0.5$ , the finite Hilbert-space analysis, the double pulse time evolution, the evolution of  $g(j)$  with  $u$ , analytic solution of the driven single-site problem, and derivation of the quadratic ep coupling term.
- [48] J. Bonča, S. A. Trugman, and I. Batistić, *Phys. Rev. B* **60**, 1633 (1999).
- [49] J. Bonča, T. Katrašnik, and S. A. Trugman, *Phys. Rev. Lett.* **84**, 3153 (2000).
- [50] L.-C. Ku, S. A. Trugman, and J. Bonča, *Phys. Rev. B* **65**, 174306 (2002).
- [51] D. Golež, J. Bonča, L. Vidmar, and S. A. Trugman, *Phys. Rev. Lett.* **109**, 236402 (2012).
- [52] J. Kogoj, M. Mierzejewski, and J. Bonča, *Phys. Rev. Lett.* **117**, 227002 (2016).
- [53] J. Bonča and S. A. Trugman, *Phys. Rev. B* **103**, 054304 (2021).
- [54] P. T. Jun and J. C. Light, *J. Chem. Phys.* **85**, 5870 (1986).